Experimental Mechanics (2022) 62:563–572
https://doi.org/10.1007/s11340-021-00795-6

RESEARCH PAPER

Study on the Effect of Scanning Strategy on Residual Stress in Laser Additive Manufacturing with the Laser Ultrasound Technique

Y. Zhan[1] · H. Xu[1] · W. Du[1] · C. Liu[2]

Received: 5 March 2021 / Accepted: 18 October 2021 / Published online: 17 November 2021

Abstract

Background During the laser additive manufacturing (LAM) process large temperature gradients can form, generating a mismatch in deformation that can lead to high level of residual stress. The stress can have irreversible effects such as warping and cracking of parts during and post manufacturing.

Objective One of the most important LAM parameters that should be controlled carefully in order to effectively manage residual stress is the scanning strategy. This study presents an evaluation of six different scanning strategies, namely reciprocating, 90° reciprocating, line, screwing, reciprocating overlapping and island scanning strategies with respect to their effect on residual stress.

Methods Laser ultrasound technology, as an advanced nondestructive testing method, is applied to measure the residual stress distribution under different scanning strategies for the first time. The surface wave generated by laser is used to evaluate the plane stress state within the surface layer of the specimen.

Results The results show that the island scanning strategy is found to contribute to the least average residual stress, and lowered residual stress by up to 45% relative to the line scanning strategy. The overall stress level is island < reciprocation overlapping < screwing < 90° reciprocating < reciprocating < line. Further to this, the effect of inspection path on the results of residual stress measurement is discussed and the concept of optimal inspection path is proposed for the first time.

Conclusions Laser ultrasound method can effectively measure the residual stress in laser additive manufacturing, and the research can serve as useful guidelines for engineers and designers to restrain and evaluate residual stress in LAM.

Keywords Laser additive manufacturing · Scanning strategy · Residual stress · Laser ultrasound

Introduction

Laser Additive Manufacturing (LAM) technique is of interest to industry due to capability of manufacturing fully functional complex geometries from a digital model by joining material in a layer by layer manner. Compared with the traditional subtractive manufacturing process, it can realize the direct forming of complex structure, high performance and compact metal components [1, 2]. However, a significant problem is the high residual stress, which is caused by high cooling rate and large temperature gradient [3]. Parts can fail during an LAM build or later in service due to the high residual stress. Due to the unclear evolution of residual stress as well as the lack of detection technology, the problem of residual stress in LAM is still not solved. Therefore, it is very important to reveal the evolution and function of residual stress in the forming process. The obvious need has motivated several residual stress measurements in additively manufactured sample using, such as mechanical relaxation technique [4, 5] as well as X-ray [6] and neutron diffraction [7, 8]. Mechanical relaxation method has poor timeliness, and it will inevitably destroy the tested sample. X-ray diffraction is sensitive to the direction of detection, and it is limited to relatively low penetration depth of X-ray beam. Neutron diffraction is limited to the cost of neutron source construction and neutron diffraction device is not portable.

Laser ultrasound is a new nondestructive testing technology which uses laser to excite and detect ultrasound. It is the

✉ Y. Zhan
zhanyu@mail.neu.edu.cn

[1] College of Sciences, Northeastern University, Shenyang 110819, China

[2] Key Laboratory for Anisotropy and Texture of Materials Ministry of Education, Northeastern University, Shenyang 110819, China

perfect combination of laser technology and ultrasound technology [9–12]. Laser ultrasound has shown strong potential over other traditional methods in the measurement of residual stress due to its advantages, such as high efficiency, high precision, non-contact, non-destructive, strong adaptability, good accessibility and *in situ* measurement. In particular, laser ultrasound technology is expected to solve many problems in the on-line measurement of residual stress in LAM, and provide reliable technical support for the rapid development of LAM technology. In recent years, many researchers have been attracted by laser ultrasound technology. Zhan et al. determined the residual stress in laser welded steel plate by laser induced surface wave. The pre-stress loading method was used to obtain the acoustoelastic coefficients [13]. Sanderson et al. studied the relationship between the velocity of laser-induced surface wave and the magnitude of residual stress, and the influence of stress distribution on test results was discussed [14]. Ruiz et al. discussed the dispersion phenomenon of laser induced surface wave due to residual stress, and the diffraction correction was introduced to improve measurement accuracy of surface wave [15]. Huan et al. used harmonic modulation and lock-in detection method to investigate the laser ultrasound signal sensitivity to the stress–strain state of ordinary aluminum alloy sample. During the tensile procedure, both amplitude and phase signals exhibited good repeatability and sensitivity to the increasing stress–strain within the elastic regime [16]. Karabutov et al. used fiber laser and PZT transducer to excite and detect the ultrasound wave, and the experiment system was applied to measurement of residual stress in electronic welding stainless steel specimen [17]. Bescond et al. measured residual stress of metal shot peening using laser generated surface skimming longitudinal wave. The influence of surface roughness can be reduced and the stress measurement accuracy can be improved [18]. Levesque et al. investigated laser ultrasound technique for residual stress measurement in friction stir welding. The residual stress distribution measured by the experiment is consistent with the results of finite element simulation [19].

Laser additive manufacturing is a complex process of multi-physical field coupling, and many process parameters affect the formation and development of the residual stress. As an important parameter, scanning strategy has attracted extensive attention, and the effects of scanning strategy on residual stress have been studied. Cheng et al. predicted lowest residual stress for LAM IN-718 component using 45° line scanning based on finite element analysis [20]. Woo et al. used directed energy deposition to manufacture five different types of specimens. The residual stress distributions were experimentally measured through the thickness of the specimens by neutron diffraction [21]. Parry et al. used a thermo-mechanical model to better understand the effect of laser scanning strategy on the generation of residual stress in selective laser melting. The greatest stress component was found to develop parallel to the scanning vectors, creating an anisotropic stress distribution in the part [22]. Mercelis et al. presented a simple theoretical model to predict the residual stress distribution. The results showed that island scanning strategy results in a reduction in residual stress and island size had no effect on residual stress [23]. Ali et al. examined the effect of scanning strategy and rescanning strategy on residual stress formation and mechanical properties of TC4 parts based on hole drilling method and finite element simulation. 90° alternating scanning strategy resulted in the lowest residual stress and re-scanning with 150% energy density resulted in 33.6% reduction in residual stress [24]. Mugwagwa et al. used the X-ray diffraction technique to measure the residual stresses under four different scanning strategies. The successive chessboard scanning strategy was found to contribute to the least average residual stresses, and lowered residual stress by up to 40% relative to the default island scanning strategy [25]. Salman et al. examined the effect of four different scanning strategies on the microstructure and mechanical behavior of 316 L stainless steel synthesized by SLM. The results indicated that the scanning strategy had negligible influence on phase formation and the residual stress had no apparent influence on the mechanical properties of the samples [26]. Patcharapit et al. developed a multiscale numerical model to predict distortion and estimate residual stress in entire parts. It was found that residual stress minimization could be achieved by using short scan vectors as it resulted in higher surface temperature and smaller temperature gradient at solidification front. The numerical result was consistent with the X-ray diffraction measurements [27]. Researchers have done a lot of work by using numerical simulation and traditional experimental methods to study the influence of scanning strategy on residual stress. However, the combination of advanced stress measurement technology and microstructure analysis is still a promising method to clarify the evolution mechanism of residual stress.

In this study, several samples are additively manufactured with six different scanning strategies, namely reciprocating, 90° reciprocating, line, screwing, reciprocating overlapping and island scanning strategies. The effect of scanning strategy on residual stress is discussed. Laser ultrasound technology, as an advanced nondestructive testing method, is applied to measure the residual stress distribution under different scanning strategies for the first time. The residual stress in TC4 samples produced by LAM is considered as plane stress state within the surface layer, and the surface wave induced by laser is used to measure the residual stress. The experimental results of laser ultrasound measurement are verified by X-ray diffraction. The results show that the longitudinal stress is obviously greater than the transverse stress, and the former is about 4 ~ 5 times of the latter in the

high stress area. The island scanning strategy is found to contribute to the least average residual stress, and lowered residual stress by up to 45% relative to the line scanning strategy. The overall stress level is island < reciprocation overlapping < screwing < 90° reciprocating < reciprocating < line. Further to this, the effect of inspection path on the results of residual stress measurement is discussed and the concept of optimal inspection path is proposed for the first time.

Theoretical Basis

Ultrasound measurement of the residual stress is based on the acoustoelastic theory. The effect of stress on the propagation of ultrasound wave is the variation in wave velocity of propagation. Generally, the change of wave velocity is proportional to the stress, and the proportional coefficient is dependent on the second-order and third-order elastic constants, which are called the acoustoelastic coefficient. The acoustoelastic effect of ultrasound surface wave was reviewed by Pao et al. [28], here only to provide the final result. Considering the study of the LAM residual stress of an isotropic and uniform part, the incident depth of the surface wave is about one wavelength, and the measured surface is a free surface without external force. Therefore, the assumption that $\sigma_z = 0$ within the surface layer of the component is adopted. In this study, the surface wave propagation on the free surface of an elastic and isotropic media defined by normal plane coordinates (x, y) is considered. When the displacement caused by the surface wave propagation is infinite, the relative change in the propagation velocity can be expressed as a function of two nonzero surface stresses,σ_x and σ_y, as follows:

$$\frac{\Delta v_x}{v_0} = \frac{v_x - v_0}{v_0} = A_x\sigma_x + A_y\sigma_y \tag{1}$$

$$\frac{\Delta v_y}{v_0} = \frac{v_y - v_0}{v_0} = A_x\sigma_y + A_y\sigma_x \tag{2}$$

In these equations, v_0 is the surface wave velocity in an unstressed medium, v_x and v_y are the surface wave velocities in the presence of (σ_x, σ_y) in the x and y directions, σ_x and σ_y are the principal stresses, and A_x and A_y are the acoustoelastic coefficients. The principle of the acoustoelastic effect calibration consists of performing a step-by-step uniaxial loading and unloading of the test specimen. The reference signal and the signal corresponding to a given load are then measured. When the sample is in a uniaxial stress state, equations (1) and (2) can be simplified as follows, respectively:

$$\frac{\Delta v_x}{v_0} = \frac{v_x - v_0}{v_0} = A_x\sigma_x \tag{3}$$

$$\frac{\Delta v_y}{v_0} = \frac{v_y - v_0}{v_0} = A_y\sigma_x \tag{4}$$

The experimental results confirmed the linear evolution of the relative variation of the velocity as a function of the load, and the slope directly corresponds to the acoustoelastic coefficients. From equations (3) and (4), for a definite prestress, if the surface wave propagation velocity along the x and y directions is measured, we obtain the acoustoelastic coefficients A_x and A_y, respectively.

Experimental Process

The whole experimental process is divided into two parts: preparation of the deposited specimens with LAM, measurement of the residual stress with laser ultrasound.

Preparation of the Deposited Specimens

Experimental equipment and process parameters

Table 1 shows the chemical composition of Ti-6Al-4 V alloy powder with a particle size of 140–200 μm from China Aviation Melt Powder Technology Co., Ltd., used in this investigation. The powder has the characteristics of uniform composition, high sphericity, hollow defect less than 2%, and oxygen content less than 0.1%. TC4 titanium alloy block is used as the substrate. The same material is used to reduce the stress and additional deformation caused by different physical properties of the material. This work is carried out on the laser melting deposition system produced by YT Proceess Engineering Ltd, as shown in Fig. 1. The system is composed of FESZL laser forming element, gas circulation purification device, sealing operation box, micro oxygen analyzer, and computer control platform. A series of single wall structures are fabricated using the process parameters as follows: laser power 500 W, scanning speed 600 mm/min, feeding rate 10.5 g/min, layer height 0.4 mm, laser path spacing 1 mm and build accuracy 0.05 mm. In the process of

Table 1 Chemical composition of TC4 powder

Element	Ti	V	Al	C	Fe	N	O
Composition(wt.%)	Bal	3.82	5.83	0.023	0.068	0.006	0.09

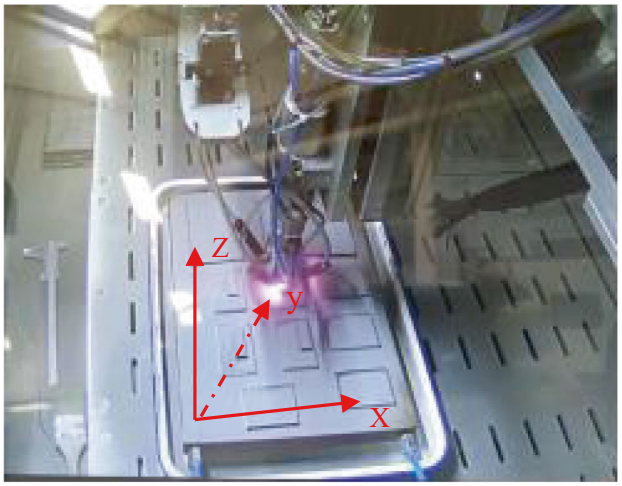

Fig. 1 The internal structure of laser melt deposition system, x axis represents scanning (longitudinal) direction, and z axis represents building (transversal) direction

pretreatment, minimize the TC4 alloy powder contact with air, so as to avoid the oxidation of titanium during printing and forming. Firstly, the laser melting deposition box is filled with high purity inert gas argon and extracted vacuum degree below5.0×10^{-2} Pa. Then, re-fill the argon and keep the pressure of laser melting deposition box is at one pressure. Finally, the dried TC4 powder is added to the powder feeder, and the pressure and flow rate of the equipment are adjusted according to the parameters required of the current experiment. The effect of scanning strategy on residual stress is determined by building six 40 mm × 15 mm × 6 mm deposited specimens for different scanning strategy, as shown in Fig. 2. After observation and screening, six specimens with excellent quality are retained to study the residual stress. Polish and rinse the *xoz* surface (15 mm × 40 mm) of the specimen until the surface is smooth and clean.

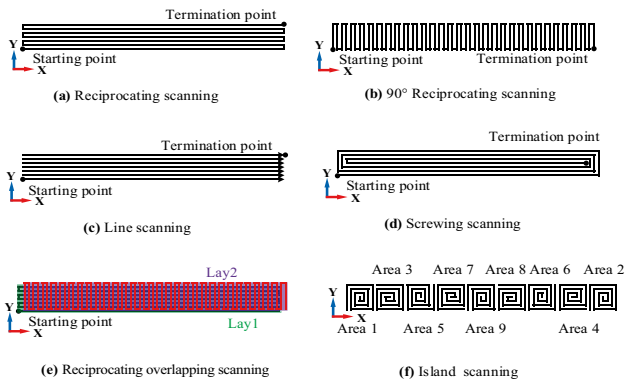

Fig. 2 The schematic diagram of different scanning strategy, (**a**) is reciprocating scanning, (**b**) is 90° reciprocating scanning, (**c**) is line scanning, (**d**) is screwing scanning, (**e**) is reciprocating overlapping scanning and (**f**) is island scanning

Microstructure

Such as the single wall specimens prepared with line and line overlapping scanning strategies, the microstructures of TC4 alloy are observed and investigated by means of optical microscope and SEM. The specimens are cut into 10 mm × 10 mm × 5 mm blocks by wire cutting and are inlaid with a paste made of denture powder and denture water. Sand the specimens with 240#, 400#, 600#, 800#, 1000#, 1500 #, 2000# and 3000# sandpaper in sequence, and then mechanical polishing is carried out in the direction perpendicular to the scratch until no scratch is observed under the optical microscope. The polishing solution is a suspension of 50 nm nano-SiO_2 and H_2O_2. Then, the specimens are etched by the Kroll reagent and are washed with anhydrous ethanol. OLYMPUS-GX71 inverted metallographic microscope made by Japan is used to observe the surface microstructure of the specimens.

Figure 3(a) shows the microstructure at 50 times magnification, and the traces left by the deposition process can be clearly observed. The white and bright banded structure is the remelting zone, and the separation zone between typical interfacial layers is clear and visible. Figure 3(b) shows a typical scaly structure, and the arc pass corresponds to the Y value in Fig. 3(c). The Y value represents the distance between laser pass, about 1 mm, which is consistent with the theoretical value. In Fig. 3(c), a large number of β columnar crystal cross section structures and traces left by laser scanning can be observed.

Figure 4 shows the microstructure of single wall specimen with line overlapping scanning strategy, due to the overlapping scanning strategy, the laser deposition forming trace is not obvious. As shown in Fig. 4(c) the columnar crystal cross section distribution is uniform and fine. On the other

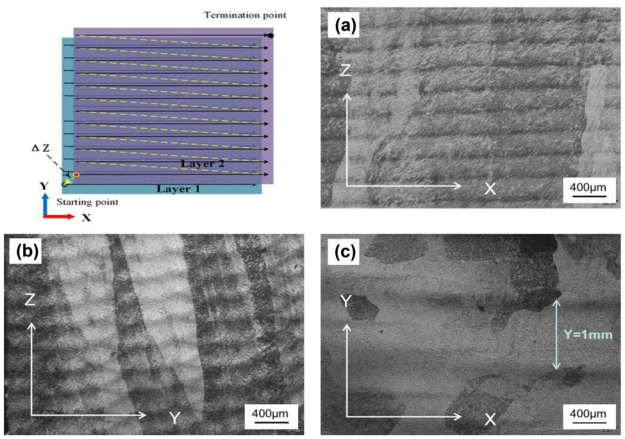

Fig. 3 Macrostructure of single wall specimen with line scanning strategy, *x* axis represents scanning direction, *y* axis represents overlap direction and *z* axis represents building direction

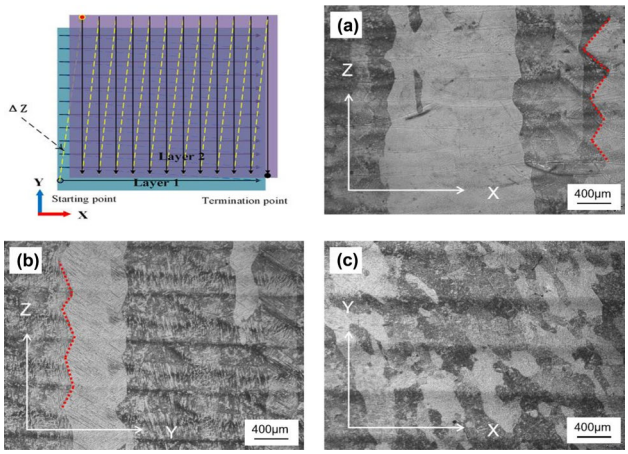

Fig. 4 Macrostructure of single wall specimen with line overlapping scanning strategy, *x* axis represents scanning direction, *y* axis represents overlapping direction and *z* axis represents building direction

hand, the growth characteristics of columnar crystals with overlapping scanning are more obvious, as shown by the red dotted line in Fig. 4(a) and (b). The columnar crystal grows against the heat flow, and the heat flow direction is not stable. The rapid melting and solidification results in a large temperature gradient, which leads to component supercooling at the front of the solid–liquid interface. Therefore, it is difficult for the grains to keep growing in the direction perpendicular to the deposition layer all the time, thus forming the zigzag pattern of about 100° as shown in Fig. 4(a).

Figure 5 shows the high-power macrostructure morphology of deposited TC4 alloy sample observed by SEM. It can be seen that the acicular martensite is distributed between the β phase, and some acicular α phases are staggered and truncated together in Fig. 5(a) and (c), which is basketweave

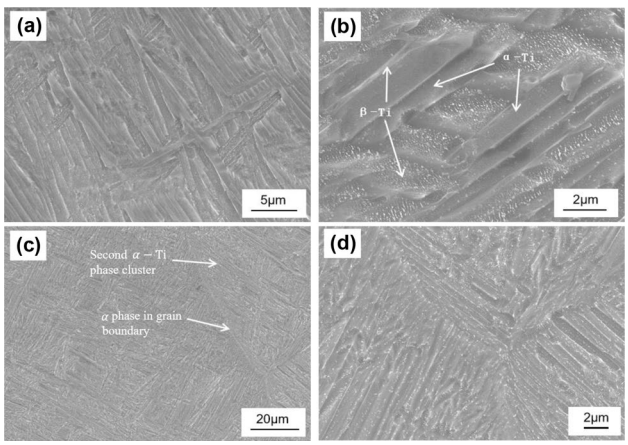

Fig. 5 Macrostructure morphology of deposited TC4 alloy sample observed by SEM, all observation points are taken at different positions in the x–y plane and x–z plane, (**a**) 3000X, (**b**) 10000X, (**c**) 1000X, (**d**) 5000X

structure. Figure 5(b) shows the macrostructure at 10,000 times. The dark gray strip structure is primary α phase, and the bright white strip between α phase is β phase or $\alpha+\beta$ phase. In Fig. 5(c), the α phase in the crystal boundary is continuous, and the secondary α phase precipitates on the grain boundary to form α phase cluster.

Laser Ultrasound for Measurement of Residual Stress

Experimental device

The laser ultrasound system is used to measure residual stress in LAM. As shown in Fig. 6, the system consists of three parts, ultrasound generating module, ultrasound detection module and stress loading apparatus. The ultrasound surface wave is generated by Nd: YAG laser equipment (Dawa-100, Beamtech Ltd., Beijing, China). The laser beam (maximum pulse energy $E_0 = 100$ mJ, wavelength $\lambda = 1064$ nm, maximum repetition frequency $f = 20$ Hz,pulse width $\tau = 8$ ns) is emit by the laser device, and focused on the surface of the specimen by a cylindrical lens to generate the ultrasound wave. The ultrasound vibration is detected by the laser Doppler vibrometer (LV-S01, Sunny Optical Technology Ltd., Suzhou, China). The He–Ne laser (wavelength 632.8 nm, frequency band 2.5 MHz, work distance 0.35 ~ 20 m, displacement resolution 0.008 nm) is emits by the vibrometer. By rotating the lens in front of the vibrometer, the detection laser can be finely adjusted and focused on into a light spot with a diameter of 0.7 mm. The photoelectric detector with the detectable wavelength range 200 ~ 1100 nm is used to realize the synchronization of laser shots and oscilloscope. The Tektronix Dpo4102 digital oscilloscope, with sampling rate 5 GS/s and bandwidth 1 GHz, is used to store the signals from photoelectric detector and laser Doppler vibrometer. The signal is averaged after 64 repetitions to improve the signal to noise ratio. The stress loading equipment is applied to calibrate the acoustoelastic constants by on-line loading. In order to avoid the mutual interference of each mode of the ultrasound wave signal, enough

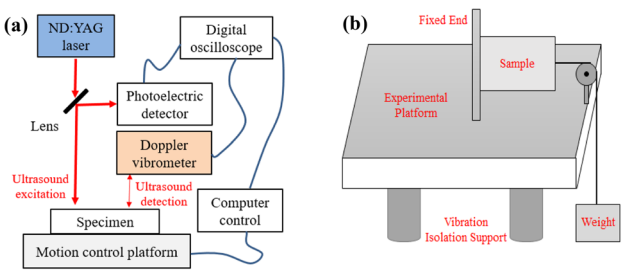

Fig. 6 Experimental system: (**a**) laser ultrasound system, (**b**) prestress loading device

space should be kept between the excitation position and the detection position so that different ultrasound waves can be separated. In addition, the high-pass filter function of the Doppler vibrometer (OUTPUT HP FILTER: DC is namely direct current, DC Block, 60 Hz, 1 kHz) is turned on to prevent the low frequency interference signal.

Determination of acoustoelastic constants

The values of the acoustoelastic constants are obtained by applying different loads on the specimen and measuring the corresponding surface wave velocity. The specimen is produced by LAM, and solution aging heat treatment is used to eliminate the initial residual stress. The size of the specimen is about 100 mm × 5 mm × 1 mm.One end of the TC4 base material specimen is fixed on the optical experiment platform with bolts. The other end of the specimen is connected with a weight, and the different stress fields can be obtained by changing the weight. According to Saint Venant Principle, the uniformly distributed stress fields are realized in the area far away from the fixed end and the loading end. First, the surface wave velocity v_0 is measured in the base material specimen without load. Then, the specimen with different stress fields is measured. The surface wave velocities v_x and v_y are obtained in the direction of parallel and vertical to the principal stress, respectively. It should be noted that the load should be reasonably controlled to avoid plastic deformation. The surface wave velocity is equal to the propagation distance divided by the travel time. The propagation distance Δl is measured by vernier caliper and the travel time Δt is recorded by oscilloscope, as shown in Fig. 7.

As shown in Fig. 7, the surface wave signal is clear and accords with the basic characteristics of surface wave. Signal one is the ultrasound vibration from laser Doppler vibrometer. Signal two is the synchronized reference signal from photoelectric detector. The travel time Δt is obtained by the cursor. The experimental data are fitted linearly to reduce measurement error. The slope of the fitting curve is the velocity of surface wave $v_0 = 2795.2$ m/s. Next, different stress fields are applied by changing the weight. For each axial loading process, the surface wave velocity in parallel and perpendicular to the loading direction is measured. By gradually loading the specimen, the relationship between tensile stress and surface wave velocity is obtained, as shown in Fig. 8. The slope is the acoustoelastic constants of the TC4 titanium alloy. Finally, the constants are determined, $A_x = -9.108 \times 10^{-6}$ MPa^{-1} and $A_y = -7.789 \times 10^{-7}$ MPa^{-1}. For most metal material, $A_x \gg A_y$ is a clear conclusion reported by Ya et al. [29]. Once the acoustoelastic constants are obtained by online loading, the residual stress can be calculated using equations (1) and (2).

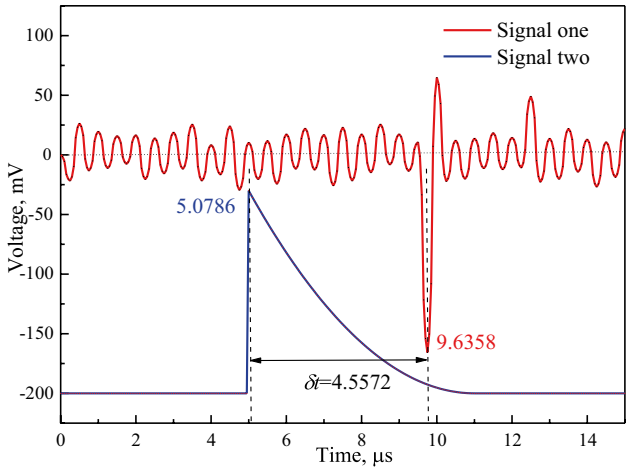

Fig. 7 Travel time of surface wave in base material specimen without load, the propagation distance is $\Delta l = 12.82$ mm, the signal one is the ultrasound signal from laser Doppler vibrometer, the signal two is the synchronized reference signal from photoelectric detector, the travel time $\delta t = 4.5572$ μs can be read by cursors

Measurement of the residual stress by laser ultrasound and X-ray diffraction

First, the residual stress in LAM TC4 specimen with line scanning strategy is measured using laser ultrasound technology. The size of the deposited specimen is about 40 mm × 15 m × 6 mm. The surface of the deposited specimen is mechanically polished to improve the intensity of the detection signal received by laser Doppler vibrometer. The polishing process is carefully controlled to ensure that there is no excessive external force. Generally, the thickness of the polished layer is less than one tenth of the incident depth of the surface wave. Figure 9 shows the

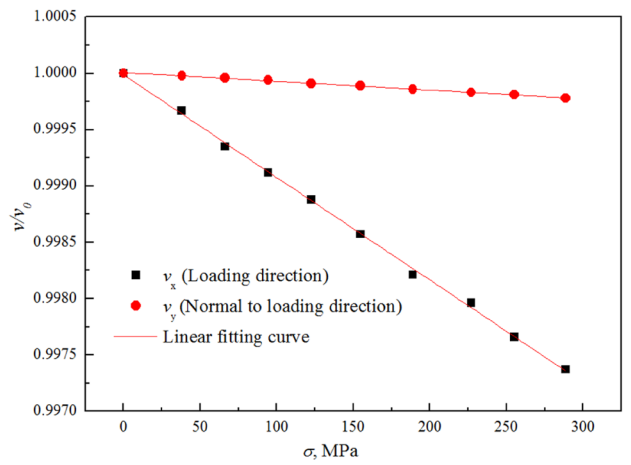

Fig. 8 The relationship between velocity ratio and applying stress. The slopes of the linear fitting curve represent the acoustoelastic constants

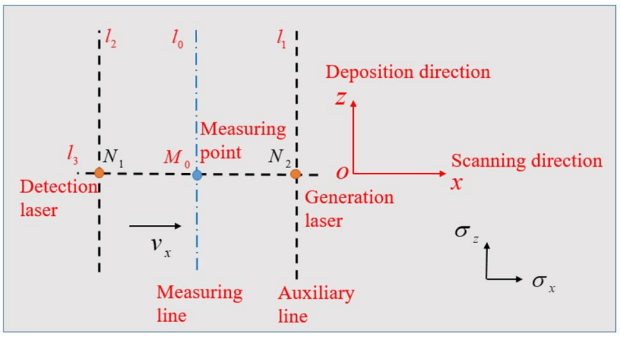

Fig. 9 Schematic diagram of measuring line arrangement for measuring the velocity v_x, M_0 is the measuring point, l_0 is the measuring line, l_1 and l_2 is the auxiliary line, N_1 and N_2 is the position of the laser irradiation

detailed measurement scheme, M_0 is the measuring point, N_1 and N_2 is the position of detection and excitation laser, σ_x and σ_z is the longitudinal and transverse residual stress, respectively. l_0 and l_3 is the measuring line, l_1 and l_2 is the auxiliary line. It should be noted that the stress at the measuring point is the mean value of the surface wave propagation distance. The vertical velocity v_z is obtained by the same experimental programs, and the residual stress of measurement point M_0 is calculated using equations (1) and (2).

Then, X-ray diffraction experiment is applied to validate the correctness of the laser ultrasound method. Usually, the stress measured by X-ray diffraction is the average value of the surface stress within tens of microns from the surface. When measuring the internal residual stress, it is necessary to peel and polish layer by layer, and the measurement result need to be corrected. The μ-X360s stress analyzer produced by Pulstec Industrial Company of Japan is used in the experiment. Five measuring points at the same position as laser ultrasound are measured, each point is measured three times, and then the average value is adopted. The residual stress measurement device is based on the cos α method. This method uses a single fixed angle of incident X-ray, usually 35° to the sample surface. All the 360° omnidirectional diffracted X-ray are sampled by a two dimensional detector in a single exposure, producing an image of the complete Debye ring. By comparing the Debye ring with stress and without stress state, the strain caused by the distortion of the diffraction ring can be obtained, and the final residual stress measurement result is automatically determined. The residual stress is evaluated using the data from the 360° omnidirectional diffracted X-ray sampled at 125 points around the Debye ring, and the residual stress is calculated by the following formula:

$$\varepsilon_{\alpha 1} = \frac{1}{2}\left\{\left(\varepsilon_{\alpha} - \varepsilon_{\pi+\alpha}\right) + \left(\varepsilon_{-\alpha} - \varepsilon_{\pi-\alpha}\right)\right\} \ (0 \le \alpha \le 2\pi) \tag{5}$$

$$\sigma_x = -\frac{E}{1+\mu} \cdot \frac{1}{\sin 2\eta} \cdot \frac{1}{\sin 2\varphi_0} \cdot \left[\frac{\partial \varepsilon_{\alpha 1}}{\partial \cos \alpha}\right] \tag{6}$$

where σ_x is the residual stress E is the elasticity modulus, μ is the Poisson ratio, η and φ_0 are the constants given by the device. $\frac{\partial \varepsilon_{\alpha 1}}{\partial \cos \alpha}$ can be obtained by linear fitting of experimental data.

Figure 10 shows the residual stress distribution in TC4 deposited specimen with laser power 500 W, feeding rate 10.5 g/min, scanning speed 600 mm/min, laser path spacing 1 mm and manufacturing time of each layer 24s. The longitudinal residual stress measured by laser ultrasound and X-ray diffraction is consistent. The laser ultrasound method obtained a larger stress than the X-ray diffraction due to the different incident depths of ultrasound surface wave and X-ray for TC4 deposited specimen. The distribution of residual stress is large in the middle and small at both ends, which is similar to an inverted bowl. It is mainly due to the stress release near the free boundary. It can be seen that the longitudinal stress is obviously greater than the transverse stress, and the former is about 5 times of the latter in the high stress area. In other words, the residual stress along the scanning direction is dominant for line scanning strategy. All the residual stress on the surface is tensile stress. The melting zone can not shrink freely during solidification and cooling, and the deformation is constrained by the surrounding area, resulting in tensile stress. The maximum longitudinal residual stress is 308.3 MPa, which is about half of the yield strength of the TC4 specimen. It should be noted that the residual stress measured is the mean value within the surface wave propagation distance. So, when the stress gradient is large, the layout of measuring point should be refined to improve the accuracy of experimental measurement.

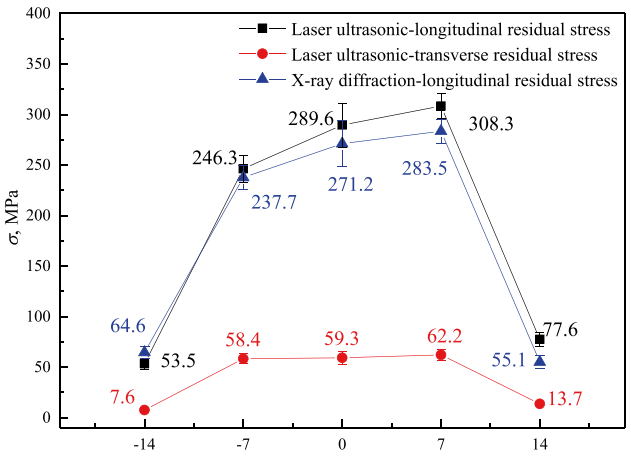

Fig. 10 The residual stress distribution along the length of TC4 deposited specimen manufactured with line scanning strategy, laser power 500 W, scanning speed 600 mm/min, feeding rate 10.5 g/min. The longitudinal residual stress is measured by laser ultrasound and X-ray diffraction

Results and Discussion

Understanding the effect of scanning strategy on residual stress is a complex problem due to the number of parameters associated with scanning strategy. Varying the size of the scanning vector length, the orientation of the scanning vectors, the order of scanning and the rotation of each subsequent layer can result in a significant combinations of scanning strategy. Here, the secondary factors are ignored, and the effect of six scanning strategies on the residual stress is discussed.

Effect of Scanning Strategy on Residual Stress

After observation and screening, six specimens with excellent quality are retained to study the residual stress. Five stress measuring points are evenly arranged on the line l_3 (as shown in Fig. 9). By sorting and calculating the experimental data, the residual stress distribution along the specimen length under each scanning strategy is obtained, as shown in Fig. 11. It can be seen that the longitudinal stress is obviously greater than the transverse stress, and the former is about 4 ~ 5 times of the latter in the high stress area. In addition to Fig. 11(e), due to the orthogonal change of scanning direction, the cumulative effect of longitudinal stress is weakened, so the stress difference between the two directions is relatively small. That is why the longitudinal residual stress is given priority in most of research on additive manufacturing. The residual stress distribution is the same in all cases discussed and the contour is like an inverted bowl. The maximum longitudinal residual stress occurs in the central region and its vicinity, and the difference between these large stresses is very small. Near the edge of the specimen, the stress decreases rapidly and the longitudinal stress at all measuring points are tensile stress. The transverse stress changes gently and compressive stress appears near the edge of the specimen. The maximum longitudinal residual stress is 308.3 MPa, which appears on line scanning strategy, and the maximum transverse stress is 69.3 MPa, which appears in reciprocating overlapping scanning strategy. The residual stress in the TC4 deposited specimens is smaller than the yield strength of the material, and it belongs to low residual stress.

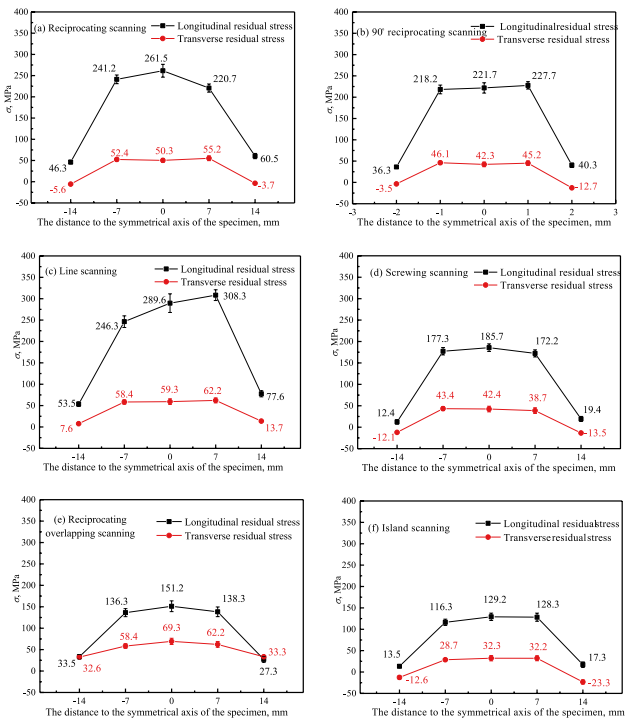

Fig. 11 The residual stress distribution along the length of TC4 deposited specimens, the specimens are produced with different scanning strategy, the longitudinal direction is defined along the scanning direction and the transverse direction is defined along the building direction

Considering the distribution of residual stress in additive manufacturing, the average values of three maximum stresses are used to evaluate the effect of scanning strategy on residual stresses, as shown in Fig. 12. The conclusion is obvious that the overall stress level is island scanning < reciprocation overlapping scanning < screwing scanning < 90° reciprocating scanning < reciprocating scanning < line scanning. In Fig. 12, the average longitudinal stress of line scan and island scan is 281.4 MPa and 124.6 MPa, respectively. The results show that the island scanning strategy is found to contribute to the least average residual stress, and lowered residual stress by up to 45% relative to the line scanning strategy. Two conclusions can be given by analyzing the results of residual stress. The first, printing components should be scanned along the short side, which can effectively reduce the residual

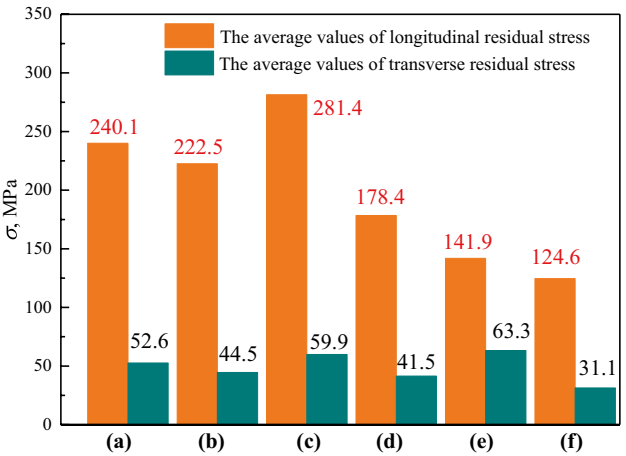

Fig. 12 The average values of the residual stress in TC4 deposited specimens with different scanning strategy, (**a**) reciprocating scanning, (**b**) 90° reciprocating scanning, (**c**) line scanning, (**d**) screwing scanning, (**e**) reciprocation overlapping scanning, (**f**) island scanning

stress. The second, if the scanning mode is not restricted, island scanning should be preferred. Reasonable zoning can largely offset the residual stress produced during additive manufacturing and also facilitate the free release of the residual stress.

Then, another five stress measuring points are evenly arranged on the auxiliary line l_1 (as shown in Fig. 9), and the longitudinal residual stress distribution along the specimen height is presented, as shown in Fig. 13. It can be seen that the integral changing tendency of residual stress is the same, regardless of which scanning strategy, the residual stress increases first and then decreases. The compressive stress is generated near the substrate due to the cooling shrinkage of the substrate. The maximum and minimum compressive stresses are 130.5 MPa and 67.5 MPa, which correspond to line scanning strategy and island scanning strategy respectively. With the increase of cladding layers, the compressive stress gradually changes into tensile stress, and the tensile stress increases with the increase of cladding layers. In the vicinity of the upper surface of the specimen, the stress is better released due to the free surface, so the tensile stress is reduced. It can be inferred that the maximum tensile stress should appear in the upper part of the specimen, about three fourths of the height.

Effect of Inspection Path on Residual Stress

Another problem that should be considered is the effect of inspection path on laser ultrasound measurement of residual stress. If the scanning strategy is known, the clear conclusion is that the inspection path of measuring residual stress along the scanning direction is preferred. But in most cases, the shape of laser additive manufacturing components is complex, and the scanning direction is often changed or unknown. It restricts us to obtain large residual stress through laser ultrasound or others experiment methods, and then evaluate the mechanical properties of the material reasonably. Therefore, the effect of different inspection path on the result of residual stress measurements is discussed here, taking linear scanning and island scanning as examples. The inspection angle θ is defined as the angle between the scanning direction and the inspection path, as shown in Fig. 14(a). M_0 is the measuring point, M_1 and M_2 is the auxiliary points, which represent the position of detection and excitation laser. Figure 14(b) shows that there is a very obvious nonlinear relationship between the stress and inspection angle. When $\theta = 0$ is expressed, the inspection path is consistent with scanning direction, and it is the most conservative method to evaluate the residual stress in LAM. In other words, the measurement along the scanning direction can avoid the laser ultrasound experimental results less than the actual stress of the measurement point in the component. With the increase of the angle, the error caused by the measurement will become larger. When $\alpha = 90$, the error between the measured value and the maximum value is the largest, and the latter is about 4 times of the former, which should be avoided. The result in Fig. 14(b) provide a new way to solve the problem mentioned above. If the residual stress in some dangerous areas of additive manufacturing component needs to be measured and evaluated, but the scanning path or the direction of principal stress is not clear, the method proposed in this paper can be used to determine the optimal inspection path.

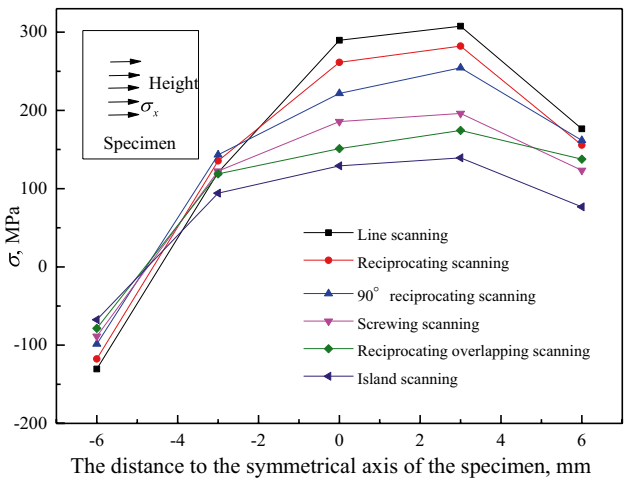

Fig. 13 The longitudinal residual stress distribution along the height of TC4 deposited specimens with different scanning strategy

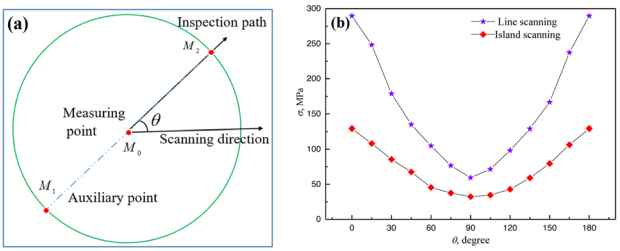

Fig. 14 The relationship between inspection angle and residual stress, (**a**) is the schematic diagram of inspection angle θ, (**b**) is the curve of experimental result

Conclusions

In this paper, laser ultrasound technology is used to measure the residual stress distribution under different scanning strategies for the first time, and the effect of scanning strategy on residual stress is discussed. The conclusion is that the longitudinal stress is obviously greater than the transverse

stress, and the former is about 4 ~ 5 times of the latter in the high stress area. The overall stress level is island < reciprocation overlapping < screwing < 90° reciprocating < reciprocating < line. The island scanning strategy is found to contribute to the least average residual stress, and lowered residual stress by up to 45% relative to the line scanning strategy. On this basis, the concept of optimal inspection path is proposed, and a new way is provided to solve the problem of unknown scanning strategy in laser ultrasound measurement of residual stress.

Acknowledgements This study is supported by the National Natural Science Foundation of China Project (Grant No. 51771051), the Natural Science Foundation of Liaoning Province Project (Grant No. 2021-MS-102) and the Fundamental Research Funds for the Central Universities (Grant No. N2105021). Meanwhile, the authors would like to thank senior engineer Su and Li of AVIC 601 Institute for helping us to complete the laser additive manufacturing experiment.

Declarations

Conflict of Interests The authors do not have any conflicts of interest to disclose and this work did not involve human or animal participants.

References

1. Gusarov AV, Grigoriev SN, Volosova MA, Melnik YA, Laskin A, Kotoban DV, Okunkova AA (2018) On productivity of laser additive manufacturing. J Mater Process Technol 261(10):213–232
2. Yan Q, Song B, Shi YS (2020) Comparative study of performance comparison of AlSi10Mg alloy prepared by selective laser melting and casting. J Mater Sci Technol 41:199–208
3. Bastian B, Florian K, Maximilian L, Roman T, Tilmann B (2020) Determination of the influence of a stress-relief heat treatment and additively manufactured surface on the fatigue behavior of selectively laser melted AISI 316L by using efficient short-time procedures. Int J Fatigue 131:105301
4. Denlinger ER, Heigel JC, Michaleris P, Palmer TA (2015) Effect of inter-layer dwell time on distortion and residual stress in additive manufacturing of titanium and nickel alloys. J Mater Process Technol 215:123–131
5. Strantza M, Vrancken B, Prime MB, Truman CE, Rombouts M, Brown DW, Guillaume P, Van HD (2019) Directional and oscillating residual stress on the mesoscale in additively manufactured Ti-6Al-4V. Acta Mater 168:299–308
6. Paul S, Singh R, Yan WY, Samajdar I, Paradowska A, Thool K, Reid M (2018) Critical deposition height for sustainable restoration via laser additive manufacturing. Sci Rep 8:14726
7. Khouzani MG, Peng H, Rogge R, Attardo R, Ostiguy P, Neidig J, Billo R, Hoelzle D, Shankar MR (2017) Experimental measurement of residual stress and distortion in additively manufactured stainless steel components with various dimensions. Mater Sci Eng A 707:689–700
8. Brown DW, Bernardin JD, Carpenter JS, Clausen B, Spernjak D, Thompson JM (2016) Neutron diffraction measurements of residual stress in additively manufactured stainless steel. Mater Sci Eng A 678:291–298
9. Zhang YJ, Wang XC, Yang Q, Dong F, Du XZ, Yin AM (2018) Characterization of mean grain size of interstitial-free steel based on laser ultrasonic. J Mater Sci 53(11):8510–8522
10. Chang Y, Yang DX, Guo YN (2018) Laser ultrasonic damage detection in coating-substrate structure via Pearson correlation coefficient. Surf Coat Technol 353:339–345
11. Yi DC, Pei CX, Liu TH, Chen ZM (2019) Inspection of cracks with focused angle beam laser ultrasonic wave. Appl Acoust 145:1–6
12. Hossam S, Miguel DP, Jose T, Ruben P, Luis R, Crina C (2020) Defect reconstruction by non-destructive testing with laser induced ultrasonic detection. Ultrasonics 101:106000
13. Zhan Y, Liu CS, Kong XW, Lin ZY (2017) Experiment and numerical simulation for laser ultrasonic measurement of residual stress. Ultrasonics 73:271–276
14. Sanderson RM, Shen YC (2010) Measurement of residual stress using laser-generated ultrasound. Int J Press Vessel Pip 87:762–765
15. Ruiz AM, Nagy PB (2002) Diffraction correction for precision surface acoustic wave velocity measurements. J Acoust Soc Am 112(3):835–842
16. Huan HT, Mandelis A, Lashkari B, Liu LX (2017) Frequency-domain laser ultrasound (FDLU) non-destructive evaluation of stress-strain behavior in an aluminum alloy. Int J Thermophys 38(4):1–11
17. Karabutov A, Devichensky A, Ivochkin A, Lyamshev M, Pelivanov I, Rohadgi U, Solomatin V, Subudhi M (2008) Laser ultrasonic diagnostics of residual stress. Ultrasonics 48(6):631–635
18. Bescond C, Monchalin JP, Gilbert A, Talbot R, Ochiai M (2005) Determination of residual stresses using laser-generated surface skimming longitudinal waves. Proc SPIE 5767:175–186
19. Levesque D, Dubourg L, Blouin A (2011) Laser ultrasonics for defect detection and residual stress measurement of friction stir welds. Nondestruct Test Evaluation 26(3):319–333
20. Cheng B, Shrestha S, Chou K (2016) Stress and deformation evaluations of scanning strategy effect in selective laser melting. Addit Manuf 12:240–251
21. Woo W, Kim DK, Kingston E, Luzin V, Salvemini F, Hill MR (2019) Effect of interlayers and scanning strategies on through-thickness residual stress distributions in additive manufactured ferritic-austenitic steel structure. Mater Sci Eng A 744:618–629
22. Parry L, Ashcroft IA, Wildman RD (2016) Understanding the effect of laser scan strategy on residual stress in selective laser melting through thermo-mechanical simulation. Addit Manuf 12:1–15
23. Mercelis P, Kruth JP (2006) Residual stresses in selective laser sintering and selective laser melting. Rapid Prototyp J 12(5):254–265
24. Ali H, Ghadbeigi H, Mumtaz K (2018) Effect of scanning strategies on residual stress and mechanical properties of selective laser melted Ti6Al4V. Mater Sci Eng A 712:175–187
25. Mugwagwa L, Dimitrov D, Matope S (2019) Evaluation of the impact of scanning strategies on residual stresses in selective laser melting. Int J Adv Manuf Technol 102:2441–2450
26. Salman OO, Brenne F, Niendorf T, Eckert J, Prashanth KG, He T, Scudino S (2019) Impact of the scanning strategy on the mechanical behavior of 316L steel synthesized by selective laser melting. J Manuf Process 45:255–261
27. Patcharapit P, Chune Y (2020) Influence of scanning length and energy input on residual stress reduction in metal additive manufacturing: Numerical and experimental studies. J Manuf Process 49:247–259
28. Pao YH, Sachse W, Fukuoka H (1984) Acoustoelasticity and ultrasonic measurement of residual stress. Academic Press, New York, pp 61–143
29. Ya M, Marquette P, Belahcene F, Lu J (2004) Residual stresses in laser welded aluminum plate by use of ultrasonic and optical methods. Mater Sci Eng A 382:257–264